

# Impact of Humidity on the CO<sub>2</sub>/N<sub>2</sub> Separation Performance of Pebax-MOF Mixed Matrix Membranes

Zikang Qin, Xuan Feng, Dengguo Yin, Bingru Xin, Ziheng Jin, Yi Deng, Lin Yang, Lu Yao, Wenju Jiang, Chong Liu,\* and Zhongde Dai\*



Cite This: *Ind. Eng. Chem. Res.* 2023, 62, 14034–14046



Read Online

ACCESS |

Metrics & More

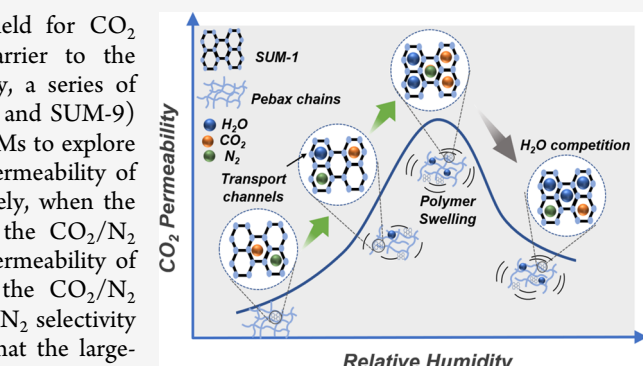
Article Recommendations

**ABSTRACT:** Postcombustion capture has been an important field for CO<sub>2</sub> capture, but its high H<sub>2</sub>O content has been a significant barrier to the performance of mixed matrix membranes (MMMs). In this study, a series of humidity values were established, and two types of MOFs (SUM-1 and SUM-9) were used in Pebax 2533 (poly(ether-block-amide)) to prepare MMMs to explore CO<sub>2</sub>/N<sub>2</sub> separation performance. At 35 °C and 2 bar, the CO<sub>2</sub> permeability of Pebax-SUM-1 was 380.9, 433.1, 405.4, and 401.7 Barrer, respectively, when the relative humidity (RH) changed from 0, 30, 60, to 100%, and the CO<sub>2</sub>/N<sub>2</sub> selectivity was 20.5, 19.0, 18.1, and 17.0, respectively. The CO<sub>2</sub> permeability of Pebax-SUM-9 was 390.9, 387.4, 412.5, and 452.4 Barrer, with the CO<sub>2</sub>/N<sub>2</sub> selectivities being 18.5, 19.9, 20.0, and 19.7, respectively. The CO<sub>2</sub>/N<sub>2</sub> selectivity had no significant fluctuations. A hypothesis has been proposed that the large-pore MOFs could only provide transport channels and could not screen CO<sub>2</sub>, and the CO<sub>2</sub>/N<sub>2</sub> selectivity would mainly be provided by the polymer matrix. Under high humidity conditions, the CO<sub>2</sub> transport channels with large-pore MOFs might fail due to competition between H<sub>2</sub>O and CO<sub>2</sub>. This study investigated the influence of a series of RH on MMMs separation performance. The proposed theory suggests that there might be an optimal humidity range for the CO<sub>2</sub> permeability of MMMs in humid conditions, which can be useful to guide the design of porous fillers for future MMMs development.

## 1. INTRODUCTION

CO<sub>2</sub> is a prevalent greenhouse gas, and its environmental impact has become increasingly critical due to economic and industrial development.<sup>1,2</sup> Carbon capture, utilization, and storage (CCUS) is a vital technology for mitigating global climate change.<sup>3,4</sup> It is noteworthy that in 2022, the CO<sub>2</sub> emissions from the power industry accounted for 39.3% of the total CO<sub>2</sub> emissions.<sup>5</sup> A significant portion of these emissions arises from fossil fuel combustion in coal-fired power plants. Postcombustion CO<sub>2</sub> capture is widely recognized as an effective approach to mitigating overall greenhouse gas emissions.<sup>6</sup> Compared with traditional CO<sub>2</sub> capture technologies such as liquid absorption,<sup>7–9</sup> solid adsorption,<sup>10,11</sup> and low-temperature distillation,<sup>12–14</sup> membrane separation has received increasing attention because of its low energy consumption, simple operation, and environmental protection.<sup>15</sup>

In previous studies, both polymeric and inorganic membranes were extensively developed for CO<sub>2</sub> capture. However, polymer membranes, despite being low-cost and readily available, face limitations imposed by the Robeson upper limit, making it challenging to achieve high permeability and selectivity simultaneously.<sup>16</sup> Conversely, numerous inorganic



membranes exhibit separation performance surpassing the Robeson upper bound.<sup>17,18</sup> However, their complex preparation, brittleness, and high cost hinder their application as CO<sub>2</sub> separation membranes. Mixed matrix membranes (MMMs) are an emerging class of membrane material that combines polymeric matrices with porous fillers with the expectation of simultaneously improving the permeability and selectivity of CO<sub>2</sub> separation membranes.<sup>19–22</sup> The ideal MMMs can fully utilize the advantages of both the polymer matrix and filler to demonstrate a CO<sub>2</sub> separation performance beyond the Robeson upper bound.

However, in practical carbon dioxide capture applications, especially in flue gas capture after combustion, water vapor is typically present in the gas stream. In general, flue gas usually contains about 12–15% CO<sub>2</sub>, 85% N<sub>2</sub>, and water vapor.<sup>23</sup> The interaction between water vapor, CO<sub>2</sub>, and the membrane,

Received: July 7, 2023

Revised: August 11, 2023

Accepted: August 14, 2023

Published: August 25, 2023



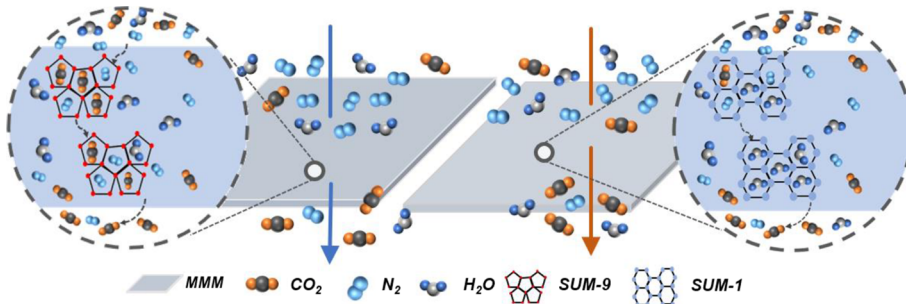


**Figure 1.** Schematic diagram of the transport mechanism for Pebax-SUMs MMMs.

along with the influence of  $\text{H}_2\text{O}$  on the  $\text{CO}_2/\text{N}_2$  separation performance of the membrane, is a subject of concern. Numerous studies have examined the impact of relative humidity (RH) on membrane  $\text{CO}_2$  separation performance, but they mainly focus on facilitated transport membranes and polymer membranes. Extensive research in the field of facilitated transport membranes has demonstrated that  $\text{H}_2\text{O}$  molecules can engage in reversible reactions with affinity  $\text{CO}_2$  groups (e.g., amino and amine groups), facilitating  $\text{CO}_2$  transport in a favorable direction.<sup>2,24</sup> In the field of polymer membranes, Dai et al.<sup>25</sup> observed an increase in  $\text{CO}_2$  permeability in a hybrid Nafion and IL (ionic liquids) membrane with rising RH. They postulated that the presence of  $\text{H}_2\text{O}$  can create nanoscale water channels within Nafion, providing a theoretical pathway for preferential gas molecule diffusion. Studies on the impact of  $\text{H}_2\text{O}$  on the  $\text{CO}_2$  separation performance of MMMs mainly focus on ternary MMMs, and functional additives are mostly amine and ammonia functional additives, where  $\text{H}_2\text{O}$  plays a role similar to that of facilitated transport membranes. However, nearly all studies investigating the impact of  $\text{H}_2\text{O}$  on MMMs separation performance are conducted under fixed RH conditions, lacking a diverse range of humidity levels to accurately assess the  $\text{H}_2\text{O}$  influence on MMMs gas separation performance.

Moreover, it is important to highlight that  $\text{CO}_2$  and  $\text{H}_2\text{O}$  strongly interact with each other, and the presence of  $\text{H}_2\text{O}$  can hydrolyze the metal–organic coordination bonds in MOFs, resulting in the degradation of the MOFs' crystalline structure.<sup>26–28</sup> For instance, Mg-MOF-74 possesses open Mg(II) sites, and when exposed to 70% RH, the  $\text{CO}_2$  uptake of Mg-MOF-74 decreased by 84%, accompanied by a significant reduction in the surface area.<sup>29–31</sup> The demanding conditions encountered in practical applications present new challenges for the stable operation of polymer-MOF MMMs. Here, we used Pebax 2533 (poly(ether-block-amide)) as the matrix, incorporated novel hydroxamate-based MOFs as the filler to prepare MMMs, and conducted groundbreaking research on the  $\text{CO}_2$  separation performance of MMMs under a series of humidity conditions, proposing the separation mechanism of large-pore MOFs under the coexistence of  $\text{CO}_2$ ,  $\text{N}_2$ , and  $\text{H}_2\text{O}$ . When the pore size of the MOFs is larger, the filler mainly provides the transport pathway, resulting in the improvement of  $\text{CO}_2$  permeability, while the  $\text{CO}_2/\text{N}_2$  selectivity is provided by Pebax 2533, which remained almost unchanged throughout our entire exploration. Furthermore, we proposed the competitive transport of  $\text{H}_2\text{O}$  and  $\text{CO}_2$ , along with the  $\text{H}_2\text{O}$  occupation of the SUM-1 pore channel, as illustrated in Figure 1. These findings can serve as valuable references for future researchers.

## 2. EXPERIMENTAL SECTION

**2.1. Materials.** Dimethyl terephthalate (99%), hydroxylamine hydrochloride ( $\geq 99\%$ ), sodium hydroxide ( $\geq 96.0\%$ ), dimethyl sulfoxide (99.0%), indium(III) nitrate trihydrate (99.0%), MeOH ( $\geq 99.0\%$ ), EtOH ( $\geq 99.7\%$ ), and Pebax 2533 were purchased from Adamas Co. Ltd. (Shanghai, China) and used as received. Ultrapure water was obtained from a Millipak Express 40 system (Merk-Millipore, Darmstadt, Germany). All reagents and solvents were used without further purification unless otherwise specified.

**2.2. Synthesis of MOFs.** **2.2.1. Preparation of 1,4-Benzenedihydroxamic Acid ( $\text{H}_2\text{-BDHA}$ ) Ligand.** The synthesis of ligand 1,4-benzenedihydroxamic acid ( $\text{H}_2\text{-BDHA}$ ) was carried out according to the procedure we previously reported.<sup>32</sup> hydroxylamine hydrochloride (180 mmol) and sodium hydroxide (360 mmol) were dissolved in 90 mL of deionized water, while dimethyl terephthalate (60 mmol) was dissolved in 100 mL of anhydrous methanol. The resulting mixture was acidified to pH 5.5 by adding approximately 90 mL of a 5 wt %  $\text{HCl}/\text{H}_2\text{O}$  solution, and the resulting white solid was collected by filtration. The solid was washed three times with deionized water, a saturated  $\text{NaHCO}_3/\text{H}_2\text{O}$  solution, and deionized water, respectively. The final product,  $\text{H}_2\text{-BDHA}$ , was dried at 100 °C in a vacuum oven for 12 h to yield a white powder.

**2.2.2. Synthesis of SUMs.** SUM-1 was prepared the same way we did before.<sup>32</sup> To prepare SUM-1, 0.03 mol of  $\text{ZrCl}_4$  was dissolved in 1 mL of DMF under sonication.  $\text{H}_2\text{-BDHA}$  was dissolved in 1 mL of DMF and sonicated for 20 min. The two solutions were mixed, followed by heating in an isothermal furnace at 120 °C for 50 min. After cooling to room temperature, the crystals were collected and washed with fresh DMF and then the solvent was exchanged with anhydrous ethanol and then dried under vacuum at 50 °C for 12 h to obtain a white powder of SUM-1. The pore size is 9.9 × 21.49 Å.

SUM-9 was prepared the same way we did before,<sup>33</sup> 0.2 mmol of  $\text{H}_2\text{-BDHA}$  and 0.085 mmol of  $\text{In}(\text{NO}_3)_3 \cdot 3\text{H}_2\text{O}$  were dissolved in a mixture of 2.0 mL of DMF and 1.2 mL of DMSO under sonication. The mixture was heated in an isothermal furnace at 80 °C for 5 days. The rod-shaped single crystals were collected, cleaned with fresh DMF, followed by solvent exchange with anhydrous ethanol, and then dried under a vacuum at 50 °C for 12 h to obtain a white powder of SUM-9. In addition, considering its rod-like structure, its effective pore size can be attributed to 6.06 Å.

**2.3. Fabrication of MMMs.** Pebax-SUMs MMMs were prepared using Pebax 2533 as the polymeric matrix and SUM-1 or SUM-9 as the filler. The specific procedure was as follows:

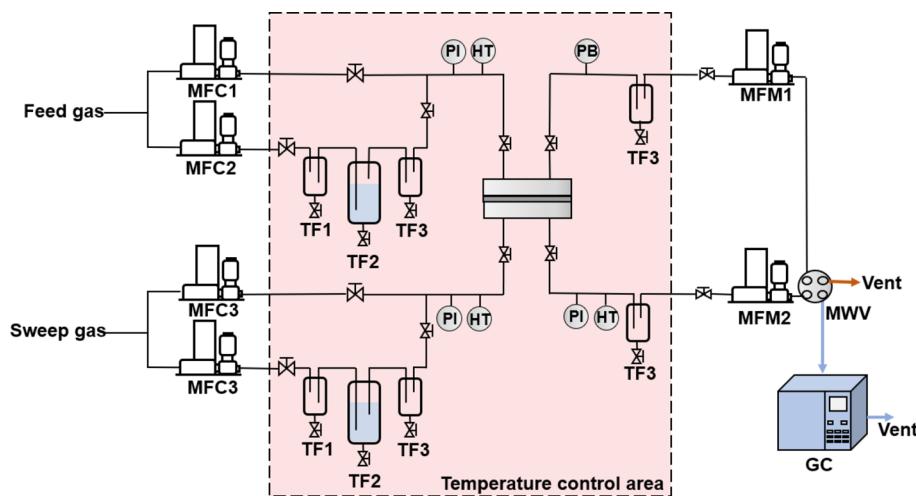


**Figure 2.** Schematic diagram of a gas mixing system. The system comprises MFC1, MFC2, MFC3, and MFC4, which are gas mass flow controllers. TF1 is a protective tank, TF2 is a water tank, and TF3 is a condensate water tank. PI and PB are pressure gauges and back-pressure valves, respectively, while HT is a humidity meter. MFM1 is a mass flow meter located at the end of the system, and the MWV is a four-way ball valve. Additionally, GC is a gas chromatograph that is used in the system.

a certain amount of Pebax 2533 was added to anhydrous ethanol, and the mixture was refluxed and stirred for 1 h at 80 °C to obtain 2 wt % Pebax 2533 solution. Then, a certain amount of SUMs was added to the solution of Pebax 2533, and the mixture was sonicated for 5 min (Ultrasonic Cell Breaker, JY88-IIIN, HUXI Industrial Co. Shanghai). The MMMs casting solution was then poured into a Teflon dish and dried overnight in an oven at 35 °C. Afterward, the MMMs were further dried in a vacuum oven at 35 °C for 12 h. It should be noted that the membrane thickness prepared was about 70 μm. For Pebax-SUM-1 MMMs, the loadings of SUM-1 were 1, 2, 5, and 15 wt %, respectively, while for Pebax-SUM-9 MMMs, the loadings of SUM-9 were 0.5, 1, 2, and 5 wt %, respectively. The loading of MMMs is calculated based on eq 1.

$$L(\text{wt}\%) = \left( \frac{M_S}{M_S + M_P} \right) \times 100\% \quad (1)$$

In which,  $M_S$  represents the mass of SUMs (g) and  $M_P$  represents the mass of Pebax (g).

**2.4. Membrane Characterization.** **2.4.1. Fourier-Transform Infrared (FTIR) Spectroscopy.** Samples were analyzed for transmittance and qualitative analysis of surface chemical bonds using a PerkinElmer Frontier FTIR spectrometer with a wavelength range of 4000–650 cm<sup>-1</sup>.

**2.4.2. Scanning Electron Microscope (SEM).** The surfaces and cross sections of the MMMs were observed using a field emission SEM (Nova Nano SEM 450, FEI, USA). The cross-sectional samples were prepared by liquid nitrogen quenching, and all samples were gold-coated before imaging.

**2.4.3. X-ray Diffraction (XRD).** The microstructure of the samples was observed using an X-ray diffractometer (XRD Ultima IV, Rigaku, Japan) with a copper target and wide-angle diffraction. The scanning range was 5–70°, the scanning speed was 5°/min, and the step size was 0.02°.

**2.4.4. Differential Scanning Calorimetry (DSC).** The basic thermal properties of the MMMs were analyzed using a differential scanning calorimeter (DSC 204 F1, Netzsch, Germany) to determine the glass transition temperatures of different MMMs. The testing procedure included three steps: first, the membrane was heated from room temperature (25

°C) to 170 °C in a high-purity N<sub>2</sub> atmosphere (99.999%) to remove water and other impurities adsorbed on the surface and inside of the membrane; then it was cooled to -150 °C and finally heated again to 170 °C with a heating/cooling rate of 10 °C/min. The third segment of the test results was selected to analyze  $T_g$  of the membrane.

**2.4.5. Thermogravimetry Analysis (TGA).** The temperature–mass relationship of the samples was analyzed using a simultaneous thermal analyzer (PerkinElmer STA 8000) to determine their thermal stability. High-purity N<sub>2</sub> gas (99.999%) was used as the carrier gas, and the testing temperature range was 30–800 °C with a heating rate of 10 °C/min.

**2.5. Gas Permeation Measurements.** Mixed gas permeation tests were performed using a mixed gas permeation testing rig (Haurp Analytical Instrument Co., Ltd., Nanjing). The feed gas consisted of a CO<sub>2</sub>/N<sub>2</sub> mixture (10/90 V/V%), while pure Ar was used as the sweep gas. The sweep gas pressure was maintained at approximately 1 bar, and the feed gas pressure was adjusted as per the desired test conditions. The operating temperature could be controlled within the range 20–75 °C. Precise control of RH (0–100%) was achieved for both the feed and sweep gas. Real-time monitoring of the gas composition on the permeation side was carried out using a gas chromatograph (GC 9790 Plus, Foley, China). A schematic diagram of the setup is shown in Figure 2.

The gas permeability ( $P_i$ ) of the  $i$ th penetrant is calculated using eq 2.<sup>34</sup>

$$P_i = \frac{N_{\text{perm}} y_i L (1 - y_{\text{H}_2\text{O}})}{A(P_{i,\text{ret}} - P_{i,\text{perm}})} \quad (2)$$

where  $N_{\text{perm}}$  represents the permeation flow rate (mL/min) measured by a soap bubble flow meter and  $y_i$  is the mole fraction (%) of gas  $i$  in the permeation flow, while  $y_{\text{H}_2\text{O}}$  represents the mole fraction of water in the permeation flow.  $L$  denotes the thickness of the membrane (μm);  $P_{i,\text{ret}}$  and  $P_{i,\text{perm}}$  are the partial pressures (bar) of gas  $i$  in the retentate and permeate, respectively, and  $A$  is the effective membrane

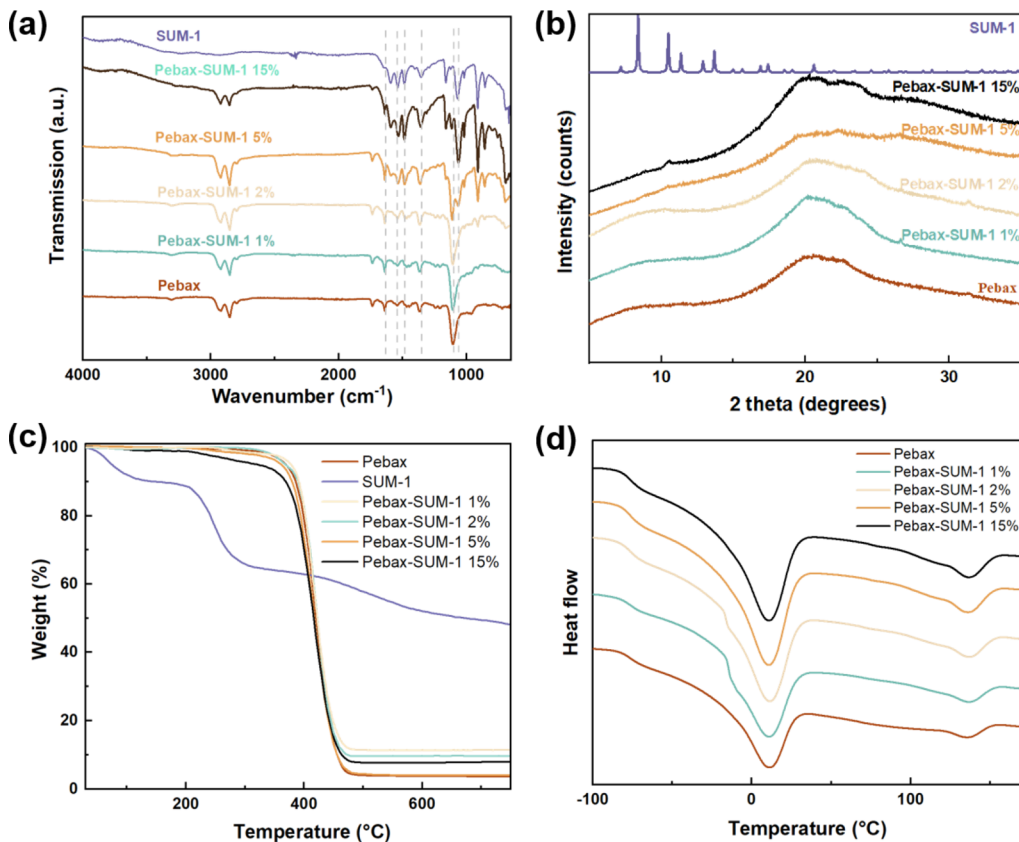


**Figure 3.** Characterization of Pebax-SUM-1 MMMs: (a) FTIR; (b) XRD; (c) TGA; and (d) DSC.

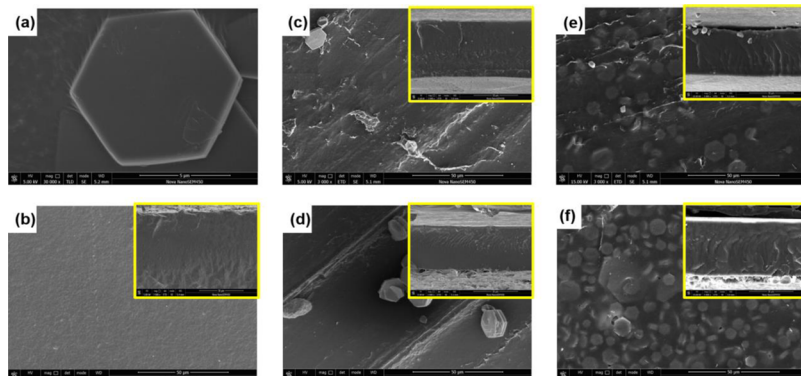


**Figure 4.** SEM images of Pebax-SUM-1 MMMs: (a) SUM-1; (b) Pebax 2533; (c) Pebax-SUM-1 1 wt %; (d) Pebax-SUM-1 2 wt %; (e) Pebax-SUM-1 5 wt %; and (f) Pebax-SUM-1 15 wt %.

area ( $\text{cm}^2$ ). In this study, the unit of gas permeability is Barrer. The separation factor is determined using eq 3.<sup>34</sup>

$$\alpha_{ij} = \frac{y_i/y_j}{x_i/x_j} \quad (3)$$

where  $y_i$  and  $y_j$  are the mole ratios of gas  $i$  and gas  $j$  in the permeate, respectively, while  $x_i$  and  $x_j$  represent the mole ratios of gas  $i$  and gas  $j$  in the retentate. All test data are obtained by averaging the measurements taken during the steady state.

**2.6. Water Vapor Uptake Tests.** Water uptake was carried out by putting the membrane in a desiccator with a RH of 100% at 35 °C. The weight of the MMM samples was measured until it reached the equilibrium state. The equilibrium water uptake was calculated according to eq 4.<sup>35</sup>

$$\text{wateruptake(wt\%)} = \frac{W_{\text{wet}} - W_{\text{dry}}}{W_{\text{dry}}} \times 100\% \quad (4)$$

where  $W_{\text{wet}}$  and  $W_{\text{dry}}$  represent the weight of the membrane at the water uptake equilibrium state and when completely dry, respectively.

### 3. RESULTS AND DISCUSSIONS

**3.1. Characterization of Membranes.** **3.1.1. Pebax-SUM-1 MMMs.** FTIR spectroscopy was used to analyze the functional groups in the prepared Pebax-SUM-1 MMMs as shown in Figure 3a. For pure Pebax membranes, Figure 3a displays a distinctive peak at  $1635 \text{ cm}^{-1}$ , which corresponds to the stretching vibration of the  $\text{C}=\text{O}$  group from the polyamide segment. Additionally, an absorption band around

**Table 1.** Thermal Properties of the Pure Membrane and Pebax-SUM-1 MMMs

sample	$T_g$ (°C)	$T_{m_{PEO}}$ (°C)	$T_{m_{PA}}$ (°C)
Pebax	-75.39	10.55	135.01
Pebax-SUM-1 1%	-75.87	10.24	136.18
Pebax-SUM-1 2%	-76.23	10.44	135.70
Pebax-SUM-1 5%	-76.27	10.88	136.41
Pebax-SUM-1 15%	-76.62	10.38	136.25

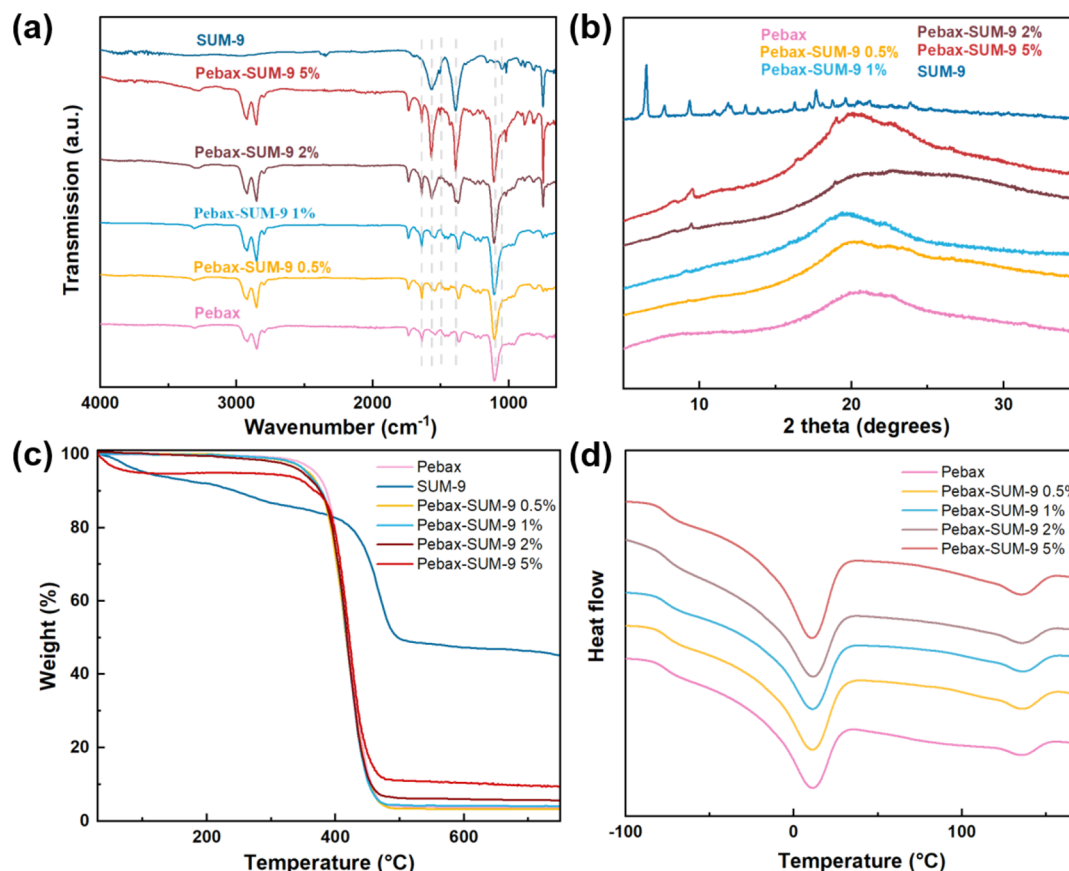
1109 cm<sup>-1</sup>, attributed to the C—O—C in the polyether portion, is observed.<sup>36,37</sup> The absorption peaks observed at 1553 and 1488 cm<sup>-1</sup> correspond to the bending and stretching vibrations of the —CNH and —C—N groups, respectively, in SUM-1, for both *cis*- and *trans*-configurations.<sup>38,39</sup> The peak at 1090 cm<sup>-1</sup> is due to the bending of the C—N bond in the C—N—O pentagon.<sup>40</sup> Notably, upon the incorporation of SUM-1 into the Pebax matrix, the aforementioned C=O and C—O peaks exhibit varying degrees of shift as the loading amounts increase (1, 2, 5, and 15 wt %). These shifts indicate the presence of hydrogen bonding interactions between —NH— and —CNH, —C—N, etc. (all of which belong to SUM-1) and Pebax. SUM-1 contains abundant C—O, so with the increase in loading amount, the absorption peak at 1399 cm<sup>-1</sup> gradually strengthens.<sup>41</sup>

Figure 3b presents the XRD analysis results of SUM-1 particles and Pebax-SUM-1 MMMs. The observed characteristic peaks closely resemble those reported in our previous studies.<sup>32</sup> In addition, in Pebax-SUM-1 MMMs, characteristic peaks of the SUM-1 crystal can be observed at a loading of 15

wt % but are not visible at lower loadings. However, the presence of SUM-1 crystals can be observed on the surface of the membrane in the SEM image in Figure 4, which may be related to the encapsulation of SUM-1 by Pebax.

The TGA curves of SUM-1 nanofiller and Pebax-SUM-1 MMMs are shown in Figure 3c. At a temperature of 200 °C, SUM-1 exhibits a weight loss of approximately 10%, while Pebax-SUM-1 MMMs show a thermal weight loss ranging from 0.5 to 1.2%, depending on the loading amount. This can be attributed to the evaporation of solvents. Beyond 200 °C and up to approximately 280 °C, SUM-1 demonstrates a continuous weight loss stage corresponding to the framework decomposition, consistent with our previous report.<sup>32</sup> Additionally, a sharp weight loss peak is observed in Pebax-SUM-1 MMMs at 450 °C, which can be attributed to the decomposition of the Pebax polymer matrix. Furthermore, we observe that with an increase in loading amount, the thermal weight loss temperature of Pebax-SUM-1 MMMs advances, consistent with the thermal degradation behavior of Pebax and SUM-1.

To analyze the interfacial interactions between SUM-1 nanoplates and Pebax 2533 membrane, pure Pebax and Pebax-SUM-1 MMMs were characterized using DSC, and the results are shown in Figure 3d and Table 1. Figure 3d depicts two primary internal heat peaks observed in all membranes, which correspond to the crystalline melting peaks of the PEO and PA segments. Notably, in Pebax-SUM-1 MMMs, the melting temperature ( $T_{m_{PEO}}$ ) of the PEO segment was found to be lower than that of pure Pebax, suggesting the presence of interactions between SUM-1 and the Pebax polymer.<sup>42</sup>

**Figure 5.** Characterization of Pebax-SUM-1 MMMs: (a) FTIR; (b) XRD; (c) DSC; and (d) TGA.

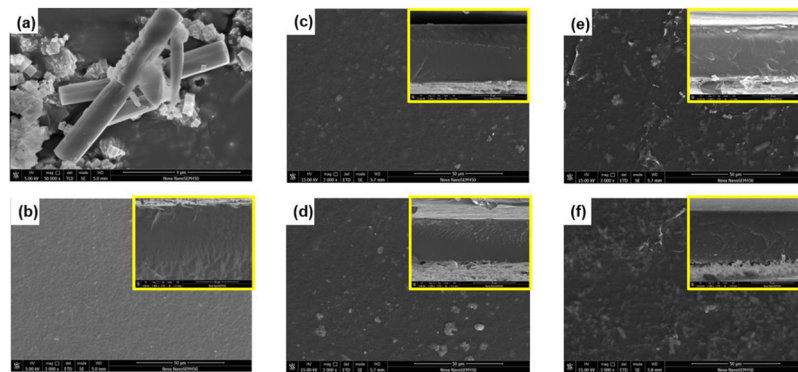


**Figure 6.** SEM images of Pebax-SUM-9 MMMs: (a) SUM-9; (b) Pebax 2533; (c) Pebax-SUM-9 0.5 wt %; (d) Pebax-SUM-9 1 wt %; (e) Pebax-SUM-9 2 wt %; and (f) Pebax-SUM-9 5 wt %.

**Table 2. Thermal Properties of the Pure Membrane and Pebax-SUM-9 MMMs**

	T <sub>g</sub> (°C)	T <sub>m</sub> <sub>PEO</sub> (°C)	T <sub>m</sub> <sub>PA</sub> (°C)
Pebax	-75.39	10.55	135.01
Pebax-SUM-9 0.5%	-75.61	10.65	135.44
Pebax-SUM-9 1%	-76.06	10.75	135.75
Pebax-SUM-9 2%	-76.66	10.86	135.45
Pebax-SUM-9 5%	-76.76	10.45	134.81

Additionally, **Table 1** presents the T<sub>g</sub> values of Pebax-SUM-1 MMMs, which were found to be lower than those of pure Pebax. This finding indicates the presence of interactions between the incorporated SUM-1 nanoplates and Pebax, leading to a restriction in the polymer chain motion of Pebax and acting as plasticizers for Pebax.<sup>43,44</sup>

The morphology of the prepared MMMs was assessed using SEM, and the results are presented in **Figure 4**. In **Figure 4a**, a typical hexagonal layered structure was observed for SUM-1, which is in good agreement with our previous study.<sup>32</sup> **Figure 4b** displays surface and cross-section SEM images of pure Pebax 2533, exhibiting a smooth structure. **Figure 4c–f** illustrates the surface morphology of MMMs with 1, 2, 5, and 15 wt % of SUM-1, respectively. The insets provide cross-sectional views of the corresponding MMMs. As can be seen from the results, the number of visible particles in the MMMs increases with increasing loading of SUM-1. Furthermore, all MMMs demonstrate good filler compatibility with Pebax 2533,

exhibiting no significant interface voids or defects. **Figure 4f** displays the 15 wt % loaded MMM, which maintains a good dispersion without agglomeration. This suggests a relatively favorable interface compatibility between SUM-1 and Pebax 2533, possibly attributed to hydrogen bonding between the –NH– groups in SUM-1 and the Pebax matrix. The cross-sectional images of the MMMs further confirm the good compatibility between SUM-1 and the MMMs.

**3.1.2. Pebax-SUM-9 MMMs.** Similar to Pebax-SUM-1 MMMs, comprehensive characterization of Pebax-SUM-9 MMMs was conducted and the results are summarized in **Figures 5** and **6**. As shown in **Figure 5a**, characteristic peaks of Pebax were observed at 1635 and 1109 cm<sup>-1</sup>.<sup>36,37</sup> The presence of SUM-9 is evidenced by the peaks observed at 1553, 1488, and 1090 cm<sup>-1</sup>.<sup>38–40</sup> However, it is noteworthy that the C–O absorption peak at 1399 cm<sup>-1</sup> gradually strengthened with increasing loading of SUM-9 (0.5, 1, 2, and 5 wt %) in Pebax-SUM-9 MMMs.<sup>41</sup> Additionally, peak shifts were observed in Pebax-SUM-9 MMMs, possibly due to the interaction between SUM-9 and Pebax 2533.

Similar observations were made in the XRD results of MMMs containing SUM-9 (**Figure 5b**). As the loading amount increases, the characteristic peak of SUM-9 in Pebax-SUM-9 MMMs becomes more prominent, while no additional peaks are detected. This observation suggests that the crystal structure of SUM-9 remains undisturbed by the Pebax 2533 surface. This suggests that Pebax-SUM-9 MMMs have the potential to maintain the structural integrity of SUM-9 while

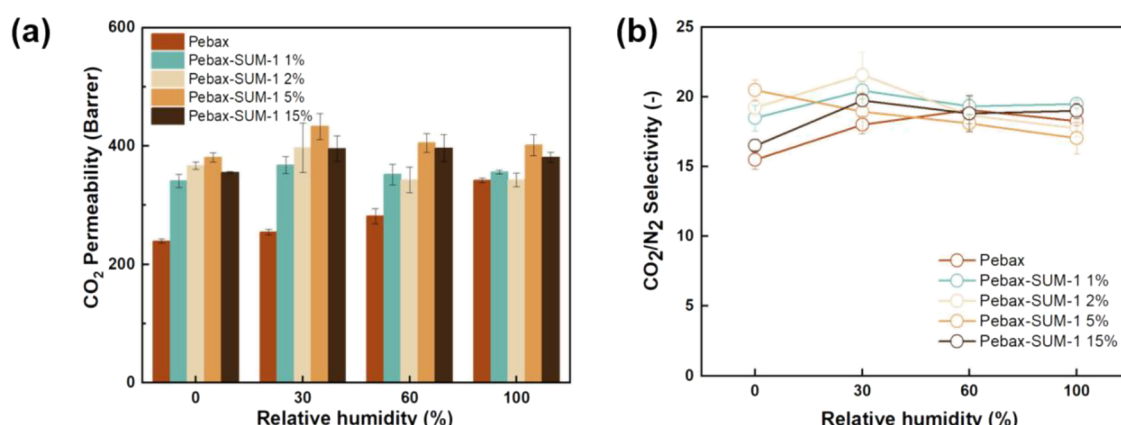


**Figure 7.** CO<sub>2</sub>/N<sub>2</sub> separation performances of Pebax-SUM-1 MMMs with different filler loadings and different RH values: (a) CO<sub>2</sub> permeability and (b) CO<sub>2</sub>/N<sub>2</sub> selectivity.

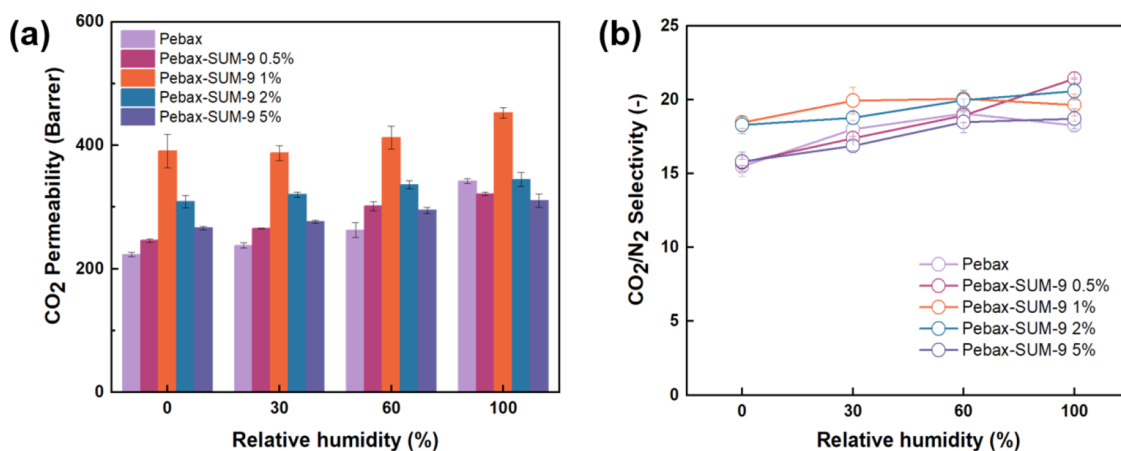


**Figure 8.** CO<sub>2</sub>/N<sub>2</sub> separation performance of Pebax-SUM-9 MMMs at different humidity conditions and loading: (a) CO<sub>2</sub> permeability of Pebax-SUM-9 MMMs at different humidity levels and loading amounts and (b) CO<sub>2</sub>/N<sub>2</sub> selectivity of Pebax-SUM-9 MMMs.

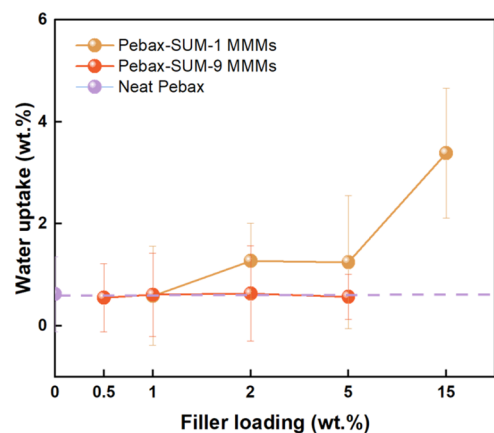


**Figure 9.** Water uptake of Pebax-SUMs at 35 °C.

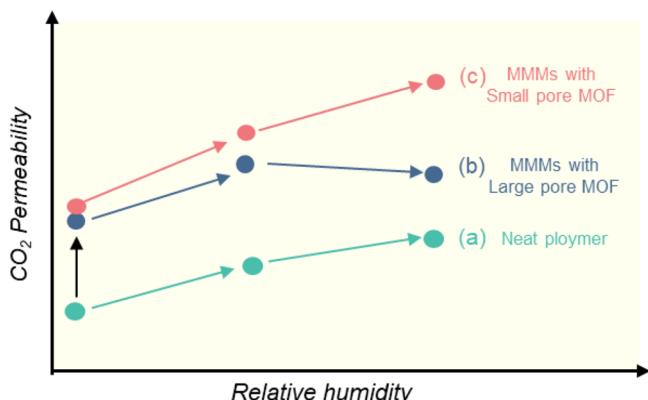


**Figure 10.** Schematic diagram of the difference in the CO<sub>2</sub> permeability trend of Pebax-SUMs with humidity changes: (a) neat Pebax membrane; (b) MMMs with large pore MOFs (i.e., SUM-1); and (c) MMMs with small pore MOFs (i.e., SUM-9).

providing enhanced properties through their synergistic combination.

Figure 5c displays the TGA curves for the SUM-9 nanofiller and Pebax-SUM-9 MMMs. At 200 °C, SUM-9 experiences a weight loss of around 10%, which can be attributed to solvent evaporation. Beyond 200 °C, SUM-9 undergoes a gradual weight loss, possibly due to (partial) framework decomposition. For Pebax-SUM-9 MMMs, the weight loss observed

around 100 °C is likely caused by solvent evaporation from the membrane and SUM-9. Notably, Pebax-SUM-9 5% exhibits a significantly pronounced weight loss during this stage. At around 450 °C, Pebax-SUM-9 MMMs exhibit a steep weight loss stage, which is attributed to significant decomposition of the Pebax polymer matrix.

DSC results of Pebax-SUM-9 MMMs are presented in Figure 5d and Table 2. It is shown that all of the membranes exhibited two main endothermic peaks, and the melting temperature (T<sub>m</sub>) of the PEO segment in Pebax-SUM-9 MMMs increased with an increase in the loading amount of SUM-9. This suggests the existence of interactions between SUM-9 and Pebax polymers.<sup>42</sup> Moreover, Table 2 demonstrates that the T<sub>g</sub> values of Pebax-SUM-9 MMMs were lower compared with pure Pebax. This indicates the presence of interactions between the incorporated SUM-9 nanosheets and Pebax, which restrict the mobility of polymer chains and act as a plasticizer for Pebax.<sup>43,44</sup>

The SEM images of Pebax-SUM-9 MMMs are shown in Figure 6, where (a) shows the crystal shape of SUM-9, which has a 1D rod-like structure. Figure 6b shows the morphology of the pure Pebax 2533 membrane. Figure 6c–f shows the morphology of MMMs loaded with 0.5, 1, 2, and 5 wt % SUM-9, respectively. Similar to Pebax-SUM-1 MMMs, the SEM image clearly shows that the MOFs dispersed nicely in the Pebax matrix without significant aggregation.

**3.2. Gas Separation Performance.** To evaluate the gas separation performance of the obtained MMMs, mixed gas permeation experiments were conducted by varying the operation parameters such as RH, operational temperature, as well as feed pressure, and the obtained results are presented in the following sections.

**3.2.1. Effect of RH.** Figure 7a,b shows the mixed gas CO<sub>2</sub>/N<sub>2</sub> separation performances of Pebax-SUM-1 MMMs with CO<sub>2</sub>/N<sub>2</sub> mixed gas (CO<sub>2</sub>/N<sub>2</sub> 10:90 V:V) as feed gas at 35 °C. The results in the figure demonstrate that the addition of SUM-1 (up to 5 wt %) substantially enhances the CO<sub>2</sub> permeability in the absence of moisture. However, increasing the SUM-1 content to 15 wt % leads to a slight decrease in CO<sub>2</sub> permeability. As observed in numerous studies,<sup>45–47</sup> increasing the gas RH value (both feed and sweep) resulted in an increase in CO<sub>2</sub> permeability for neat Pebax membranes. However, an intriguing finding is that for Pebax-SUM-1 MMMs, increasing the RH value leads to a nonlinear variation

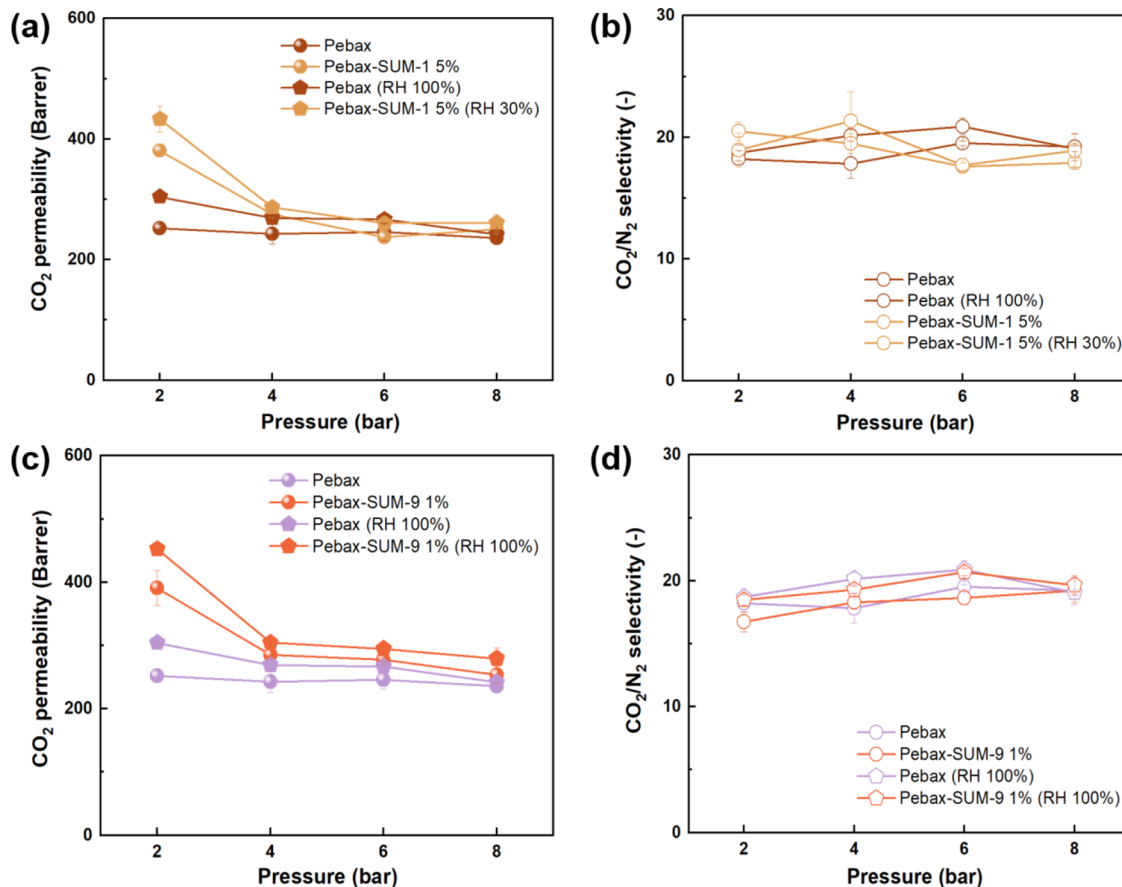


**Figure 11.** CO<sub>2</sub>/N<sub>2</sub> separation performance of Pebax-SUMs MMMs at different pressures: (a) CO<sub>2</sub> permeability of Pebax-SUM-1 MMMs; (b) CO<sub>2</sub>/N<sub>2</sub> selectivity of Pebax-SUM-1 MMMs; (c) CO<sub>2</sub> permeability of Pebax-SUM-9 MMMs; and (d) CO<sub>2</sub>/N<sub>2</sub> selectivity of Pebax-SUM-9 MMMs.

in CO<sub>2</sub> permeability. For instance, a CO<sub>2</sub> permeability of 433.1 Barrer coupled with a CO<sub>2</sub>/N<sub>2</sub> selectivity of 19.0 was observed at an RH value of 30%, while increasing the RH value to 100% resulted in a CO<sub>2</sub> permeability of only 401.7 Barrer. A similar trend was observed for all the Pebax-SUM-1 MMMs. As the reported pore size of SUM-1 was 9.9 × 21.49 Å, the reason for this may be that the H<sub>2</sub>O molecules occupy the SUM-1 pores, thus, reducing the CO<sub>2</sub> transport pathway. Considering the CO<sub>2</sub>/N<sub>2</sub> selectivity, they are less sensitive to the RH value changes.

The gas permeation properties of Pebax-SUM-9 MMMs were also investigated and are presented in Figure 8a,b. Similar to Pebax-SUM-1 MMMs, the addition of SUM-9 enhanced the CO<sub>2</sub>/N<sub>2</sub> separation performance of the MMMs in a dry state; compared to Pebax-SUM-1 MMMs, the presence of SUM-9 seems to be more effective in promoting CO<sub>2</sub> transport, and Pebax-SUM-9 MMMs with 1 wt % loading exhibit the best CO<sub>2</sub>/N<sub>2</sub> separation performance, with a CO<sub>2</sub> permeability of 390.9 Barrer and a CO<sub>2</sub>/N<sub>2</sub> selectivity of 16.7. In contrast to the Pebax-SUM-1 MMMs, the CO<sub>2</sub> permeability of each SUM-9 loading continuously increases with the RH values. For Pebax-SUM-9 MMMs with different loadings at a fixed RH, the CO<sub>2</sub> permeability always peaked at 1 wt %. In addition, the CO<sub>2</sub>/N<sub>2</sub> selectivity also exhibited an increasing trend as the RH value increased from 0 to 100% (as shown in Figure 8b). For example, at 100% RH, a CO<sub>2</sub> permeability of 452.4 Barrer, with a CO<sub>2</sub>/N<sub>2</sub> selectivity of 18.5, was recorded.

In previous studies investigating the effect of water vapor on MMMs gas separation performances,<sup>48</sup> the hydrophobicity and hydrophilicity of the nanofiller was the key parameter to lead the influence of the water vapor to be positive or negative. Hence, we conducted water vapor uptake experiments as part of this study, and the findings are presented in Figure 9. The water uptake for SUM-9-based MMMs is rather similar to pure Pebax membranes, which is around 1 wt %, and it is consistent with our previous water uptake results.<sup>49</sup> However, the water uptake is higher in the case of Pebax-SUM-1 MMMs and gradually increases with an increase in the MOFs loading. For instance, when SUM-1 loading was 5 wt % in the MMMs, a water uptake value of 1.24 wt % was documented, which is 2.21 times of the Pebax-SUM-9 MMMs. Interestingly, the water uptake trend observed in the MMMs contradicts the CO<sub>2</sub> permeability results. Higher water uptake or increased hydrophilicity does not result in higher CO<sub>2</sub> permeability.

Considering that both SUMs ligands are H<sub>2</sub>-BDHA, the BET surfaces of the two MOFs are also rather close (SUM-1 is 1252.5 m<sup>2</sup> g<sup>-1</sup>, while that of SUM-9 is 1016.3 m<sup>2</sup> g<sup>-1</sup>), and it seems that the effective oriented pore size of the fillers (theoretical values: SUM-1 9.9 Å, SUM-9 6.06 Å) might be a significant factor contributing to the significant difference in water uptake as well as the CO<sub>2</sub> permeability properties.

Based on the results obtained for Pebax-SUM-1 and Pebax-SUM-9 MMMs, possible mechanisms of influence of RH on MMMs were proposed and are presented in Figure 10. For neat Pebax membranes, the presence of H<sub>2</sub>O vapor increases

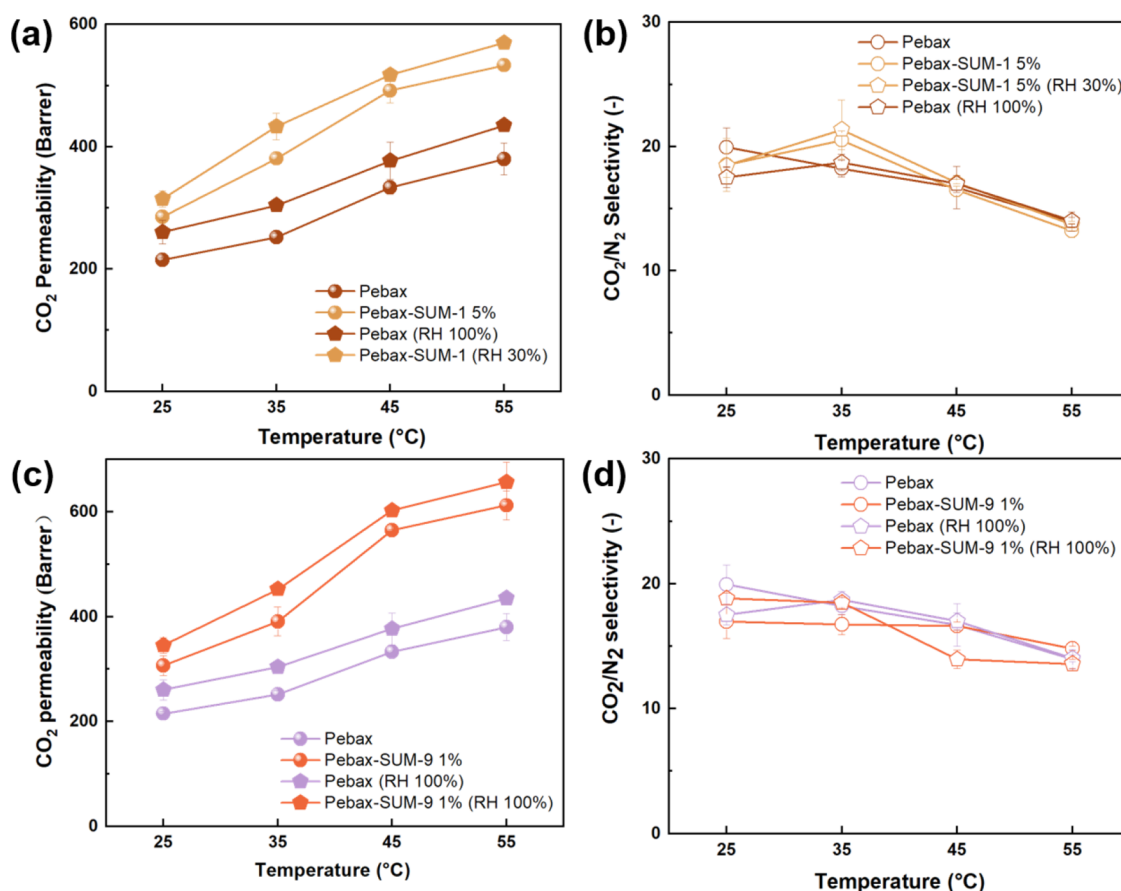


**Figure 12.** CO<sub>2</sub>/N<sub>2</sub> separation performance of Pebax-SUMs MMMs under optimal humidity conditions: (a) CO<sub>2</sub> permeability of Pebax-SUM-1 MMMs; (b) CO<sub>2</sub>/N<sub>2</sub> selectivity of Pebax-SUM-1 MMMs; (c) CO<sub>2</sub> permeability of Pebax-SUM-9 MMMs; and (d) CO<sub>2</sub>/N<sub>2</sub> selectivity of Pebax-SUM-9 MMMs.

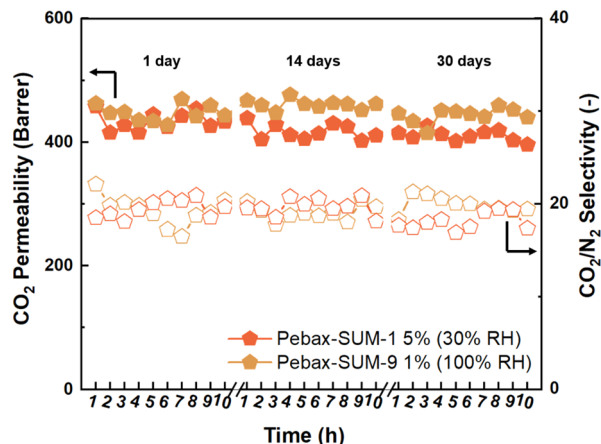


**Figure 13.** Long-term stability testing of Pebax-SUM-1 5 wt % and Pebax-SUM-9 1 wt % MMMs under a humid environment.

the activity of the PEO segment, swells the Pebax polymeric chain, and promotes an increase in the CO<sub>2</sub> permeability. This is illustrated in Figure 10a.

In the case of Pebax-SUM-9 MMMs, the CO<sub>2</sub> permeability increased with RH values. It is hypothesized that the relatively small pore structure and interlayer size of SUM-9 make it difficult for H<sub>2</sub>O molecules to enter its interior; therefore, they do not compete with CO<sub>2</sub> for the transport paths. In contrast, for Pebax-SUM-1 MMMs, the larger pore size of SUM-1 makes it relatively easy for H<sub>2</sub>O molecules to enter its pores.

Under high RH conditions, the pores of SUM-1 are gradually occupied by H<sub>2</sub>O molecules (higher water vapor uptake), thus the transport channels were blocked, leading to a reduction in CO<sub>2</sub> permeability, shown in Figure 10b,c.

**3.2.2. Effect of Feed Pressure.** Based on the results obtained in Section 3.2.1, Pebax, Pebax-SUM-1 5 wt %, and Pebax-SUM-9 1 wt % were selected to investigate the impact of feed pressures on the CO<sub>2</sub>/N<sub>2</sub> separation performance. The results are listed in Figure 11. It is found that as the feed pressure increases, the CO<sub>2</sub> permeability of the pure Pebax membrane (both dry and 100% RH conditions) remains almost unchanged, denoting that Pebax is a stable CO<sub>2</sub> separation material. In contrast, both Pebax-SUM-1 and Pebax-SUM-9 MMMs exhibit a notable decrease in CO<sub>2</sub> permeability as the feed pressure rises from 2 to 8 bar, irrespective of the presence of moisture. For instance, at 30% RH conditions, the CO<sub>2</sub> permeability of Pebax-SUM-1 decreases from 433.1 to 260.8 Barrer as feed pressure increased from 2 to 8 bar, while for Pebax-SUM-9 MMMs, the CO<sub>2</sub> permeability decreases from 452.4 to 279.3 Barrer as feed pressure increased from 2 to 8 bar. One plausible explanation for this phenomenon is that the polymer plasticizes when the membrane is exposed to higher partial pressures of CO<sub>2</sub>, thereby reducing CO<sub>2</sub> permeability.<sup>50</sup>

**3.2.3. Effect of Testing Temperature.** Similar to the previous section, the membranes with the best separation performances were selected to further investigate the testing temperature. The changes in CO<sub>2</sub> permeability and CO<sub>2</sub>/N<sub>2</sub> selectivity of Pebax and Pebax-SUM-1 5 wt % under various

**Table 3.** CO<sub>2</sub>/N<sub>2</sub> Separation Performance Comparison of Pebax 2533-SUMs MMMs with Others

MMMs	Operating conditions	P <sub>CO<sub>2</sub></sub> (Barrer)	$\alpha_{CO_2/N_2} (-)$	ref
Pebax 2533-ZIF-7-OH	23 wt %, 25 °C, 4.5 bar, single	323.0	13.7	51
Pebax 2533-ZIF-7-OH	2 wt %, 25 °C, 4.5 bar, single	249.0	32.5	
Pebax 2533-Cloisite 15A	4 wt %, 24 °C, 2 bar, single	180.0	28.0	52
Pebax 2533-ZIF-11	70 wt %, 20 °C, 2 bar, single	402.9	28.0	53
Pebax 2533-PEG-POSS	30 wt %, 40 °C, 10 bar, single	392.4	22.8	54
Pebax 3533-MIL-178	15 wt %, 35 °C, 1 bar, mixed gas	275.0	19.0	55
Pebax 1657-CNT NF	60 wt %, 25 °C, 2 bar, single	350.0	20.9	56
Pebax-ZIF-8	20 wt %, RT, 2 bar, mixed gas	227.0	25.0	34
Pebax 2533	35 °C, 2 bar, dry, mixed gas	239.3	15.5	this work
Pebax 2533	35 °C, 2 bar, 100% RH, mixed gas	339.3	18.3	this work
Pebax 2533-SUM-1	5 wt %, 35 °C, 2 bar, dry, mixed gas	380.9	20.5	this work
Pebax 2533-SUM-1	5 wt %, 35 °C, 2 bar, 30% RH, mixed gas	433.1	19.0	this work
Pebax 2533-SUM-1	5 wt %, 35 °C, 2 bar, 60% RH, mixed gas	405.4	18.1	this work
Pebax 2533-SUM-1	5 wt %, 35 °C, 2 bar, 100% RH, mixed gas	401.7	17.0	this work
Pebax 2533-SUM-9	1 wt %, 35 °C, 2 bar, dry, mixed gas	390.9	18.5	this work
Pebax 2533-SUM-9	1 wt %, 35 °C, 2 bar, 30% RH, mixed gas	395.4	19.9	this work
Pebax 2533-SUM-9	1 wt %, 35 °C, 2 bar, 60% RH, mixed gas	412.5	20.1	this work
Pebax 2533-SUM-9	1 wt %, 35 °C, 2 bar, 100% RH, mixed gas	452.4	19.7	this work

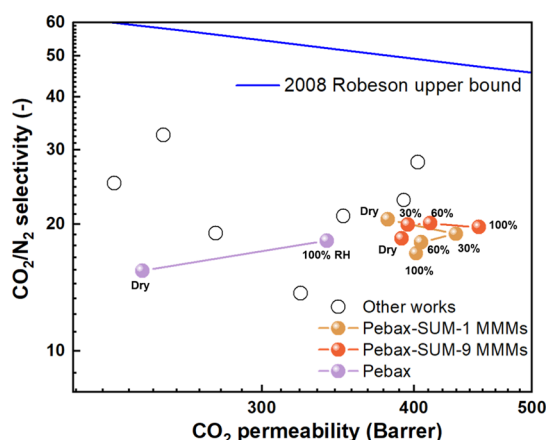


**Figure 14.** Comparison of Pebax-SUMs MMMs with other works.

operating temperatures (at a feed pressure of 2 bar) are presented in Figure 12a,b. The results indicate an increase in the CO<sub>2</sub> permeability of the MMMs with rising temperatures. The most significant increase was observed for Pebax at 100% RH, where the CO<sub>2</sub> permeability increased from 260.3 Barrer at 25 °C to 435.0 Barrer at 55 °C. For Pebax-SUM-1 5 wt % at 30% RH, the CO<sub>2</sub> permeability increased from 314.9 Barrer at 25 °C to 570.0 Barrer at 55 °C. Nevertheless, the CO<sub>2</sub>/N<sub>2</sub> selectivity of Pebax decreased from 17.5 to 14.0, and that of

Pebax-SUM-1 5 wt % decreased from 18.5 to 13.7. This may be due to the increased thermal mobility of polymer chains when the temperature changes from 25 to 55 °C, which produces additional free volume in the membrane matrix, increasing the diffusion coefficients of both CO<sub>2</sub> and N<sub>2</sub>. At the same time, high temperature is not conducive to the dissolution of CO<sub>2</sub> in Pebax, leading to a decrease in the CO<sub>2</sub>/N<sub>2</sub> selectivity. The same phenomenon was observed in the testing of Pebax-SUM-9 1 wt % MMMs. Under 100% RH, the CO<sub>2</sub> permeability increased from 345.0 to 656.8 Barrer when the temperature changed from 25 to 55 °C, and the CO<sub>2</sub>/N<sub>2</sub> selectivity decreased from 18.8 to 13.6 shown in Figure 12c,d. The reason for the change is the same as that for the Pebax-SUM-1 MMMs.

**3.2.4. Long-Term Stability.** By the synthesis of multiple batches of Pebax-SUMs MMMs and comparison of their separation performance under identical conditions, the reproducibility of the separation results was confirmed. In the long-term stability test, the gas separation performances were tested for about 10 h (steady state) and then the membrane was stored at ambient conditions between each test. The long-term stability test was carried out over a period of 30 days. Specifically, Pebax-SUM-1 with 5 wt % (30% RH) and Pebax-SUM-9 with 1 wt % (100% RH) were selected to assess their long-term stability, and the corresponding results can be found in Figure 13. The Pebax-SUMs MMMs synthesized in this study exhibited excellent and sustained CO<sub>2</sub> permeability and CO<sub>2</sub>/N<sub>2</sub> selectivity, without any noticeable decline during continuous testing under a humid environment at 2 bar and 35 °C. These findings suggest that Pebax-SUMs MMMs hold significant potential for practical applications in CO<sub>2</sub> capture within humid environments.

**3.2.5. Comparison of Membrane Performance.** Compared to our test results with other reported CO<sub>2</sub>/N<sub>2</sub> separation performances of Pebax MMMs, as shown in Table 3 and Figure 14, Table 3 presents the CO<sub>2</sub>/N<sub>2</sub> separation performance of Pebax MMMs and a comparison to our Pebax-SUMs. It can be observed that our Pebax-SUMs MMMs exhibit significant improvements in CO<sub>2</sub> permeability compared with the performance of other MMMs.

In addition, we illustrated the CO<sub>2</sub>/N<sub>2</sub> separation performance data mentioned in Table 3 graphically, as shown in Figure 14. Notably, the addition of SUMs resulted in a substantial increase in the CO<sub>2</sub> permeability of the MMMs. Specifically, the CO<sub>2</sub> permeability of Pebax-SUM-1 (5 wt %) and Pebax-SUM-9 (1 wt %) increased from 223.4 Barrer for pure Pebax to 380.9 and 390.9 Barrer, respectively, while the CO<sub>2</sub>/N<sub>2</sub> selectivity remained almost unchanged. This discovery supports our hypothesis that in the presence of relatively large filler pore sizes, the polymer matrix primarily determines the CO<sub>2</sub>/N<sub>2</sub> selectivity. Moreover, with increasing humidity, the CO<sub>2</sub> permeability of Pebax-SUM-1 (5 wt %) exhibited an upward trend, rising from 380.9 to 433.1 Barrer. However, at an RH of 60%, a decline in the CO<sub>2</sub> permeability was observed. In addition, the CO<sub>2</sub> permeability of Pebax-SUM-9 1 wt % increased from 390.9 to 452.4 Barrer with increasing RH. It is worth noting that the CO<sub>2</sub>/N<sub>2</sub> selectivity of both of these MMMs did not change significantly, and the reasons for these changes are explained in Section 3.2.1.

## 4. CONCLUSIONS

In this study, we established a series of RH measurements to test the CO<sub>2</sub>/N<sub>2</sub> separation performance of Pebax-MOF

MMMs under mixed gas conditions. FTIR confirmed improved interfacial compatibility between the MOFs, namely SUM-1/SUM-9, and Pebax 2533, which can be attributed to hydrogen bonding interactions between filler and matrix and improved contact area. SEM and XRD tests indicated that the morphology and crystal structure of MOFs remained unchanged after preparing MMMs. DSC results showed that MOFs acted as plasticizers for Pebax.

Under dry mixed gas conditions, the CO<sub>2</sub> permeability of Pebax-SUM-1 MMMs was 380.87 Barrer at 35 °C and 2 bar, 70.4% higher than that of pure Pebax, with a CO<sub>2</sub>/N<sub>2</sub> selectivity of 20.5. Pebax-SUM-9 exhibited a CO<sub>2</sub> permeability of 390.9 Barrer, 75.0% higher than that of pure Pebax, with a CO<sub>2</sub>/N<sub>2</sub> selectivity of 16.7. However, the CO<sub>2</sub>/N<sub>2</sub> separation performance of Pebax-MOF exhibited different trends as RH increased. For instance, the CO<sub>2</sub> permeability of Pebax-SUM-1 MMMs first increased and then decreased with increasing RH, while that of Pebax-SUM-9 MMMs increased with increasing RH. At 35 °C and 2 bar, the CO<sub>2</sub> permeability of Pebax-SUM-1 was 433.1 Barrer at 30% RH, with a CO<sub>2</sub>/N<sub>2</sub> selectivity of 21.9, 89.4, and 41.2% higher than that of pure Pebax, respectively. At 100% RH, Pebax-SUM-9 exhibited a CO<sub>2</sub> permeability of 452.4 Barrer and a CO<sub>2</sub>/N<sub>2</sub> selectivity of 18.5, 103.5, and 19.2% higher than that of pure Pebax, respectively. The different trends may be attributed to the distinct pore structures of SUMs, which result in competition between H<sub>2</sub>O and CO<sub>2</sub> molecules during transport. Our results also indicate that the presence of impurity gas molecules may significantly affect the CO<sub>2</sub> separation performance of MMMs, particularly when MOF pore sizes are relatively large and the CO<sub>2</sub> separation selectivity of MMMs will mainly come from the polymer matrix. In future MMMs research, especially for those with large pore sizes, the influence of impurity gases cannot be ignored.

It is noteworthy that, to the best of our knowledge, the present study is the first report on the effect of a series of humidity conditions on the CO<sub>2</sub> separation performance of MMMs. According to our performance analysis, when the pore size of the filling material is large, the CO<sub>2</sub> separation selectivity may mainly come from the polymer matrix. We hope that future research will consider the influence of impurity gases on MMM performance evaluations and closely monitor the effects of H<sub>2</sub>O molecules when testing the CO<sub>2</sub> separation performance of MMMs in humid environments.

## AUTHOR INFORMATION

### Corresponding Authors

**Chong Liu** — School of Chemical Engineering, Sichuan University, Chengdu 610065, China;  [orcid.org/0000-0002-9780-9062](https://orcid.org/0000-0002-9780-9062); Email: [liuchong@scu.edu.cn](mailto:liuchong@scu.edu.cn)

**Zhongde Dai** — National Engineering Research Centre for Flue Gas Desulfurization, Chengdu 610065, China; Carbon Neutral Technology Innovation Center of Sichuan, Chengdu 610065, China; College of Carbon Neutrality Future Technology, Sichuan University, Chengdu 610065, China;  [orcid.org/0000-0002-3558-5403](https://orcid.org/0000-0002-3558-5403); Email: [zhongde.dai@scu.edu.cn](mailto:zhongde.dai@scu.edu.cn)

### Authors

**Zikang Qin** — College of Architecture and Environment, Sichuan University, Chengdu 610065, China

**Xuan Feng** — School of Chemical Engineering, Sichuan University, Chengdu 610065, China

**Dengguo Yin** — DongFang Boiler Co., Ltd., Chengdu 611731, China

**Bingru Xin** — School of Chemical Engineering, Sichuan University, Chengdu 610065, China

**Ziheng Jin** — National Engineering Research Centre for Flue Gas Desulfurization, Chengdu 610065, China; Carbon Neutral Technology Innovation Center of Sichuan, Chengdu 610065, China; College of Carbon Neutrality Future Technology, Sichuan University, Chengdu 610065, China

**Yi Deng** — DongFang Boiler Co., Ltd., Chengdu 611731, China; Clean Combustion and Flue Gas Purification Key Laboratory of Sichuan Provincial, Chengdu 611731, China

**Lin Yang** — National Engineering Research Centre for Flue Gas Desulfurization, Chengdu 610065, China; Carbon Neutral Technology Innovation Center of Sichuan, Chengdu 610065, China; College of Carbon Neutrality Future Technology, Sichuan University, Chengdu 610065, China;  [orcid.org/0000-0002-3367-244X](https://orcid.org/0000-0002-3367-244X)

**Lu Yao** — National Engineering Research Centre for Flue Gas Desulfurization, Chengdu 610065, China; Carbon Neutral Technology Innovation Center of Sichuan, Chengdu 610065, China; College of Carbon Neutrality Future Technology, Sichuan University, Chengdu 610065, China;  [orcid.org/0000-0003-2743-758X](https://orcid.org/0000-0003-2743-758X)

**Wenju Jiang** — National Engineering Research Centre for Flue Gas Desulfurization, Chengdu 610065, China; Carbon Neutral Technology Innovation Center of Sichuan, Chengdu 610065, China; College of Carbon Neutrality Future Technology, Sichuan University, Chengdu 610065, China;  [orcid.org/0000-0003-1327-7159](https://orcid.org/0000-0003-1327-7159)

Complete contact information is available at:  
<https://pubs.acs.org/10.1021/acs.iecr.3c02308>

### Notes

The authors declare no competing financial interest.

## ACKNOWLEDGMENTS

This work acknowledges the financial support from the Sichuan Science and Technology Program (2021YFH0116), the National Natural Science Foundation of China (No. 52170112), and DongFang Boiler Co., Ltd. (3522015).

## REFERENCES

- (1) McNutt, M. Time's up, CO<sub>2</sub>. *Science* **2019**, *365* (6452), 411.
- (2) Chen, S.; Hu, G.; Smith, K. H.; Mumford, K. A.; Zhang, Y.; Stevens, G. W. Kinetics of CO<sub>2</sub> Absorption in an Ethylethanolamine Based Solution. *Ind. Eng. Chem. Res.* **2017**, *56* (43), 12305–12315.
- (3) Liu, L.; Lee, J. H.; Han, S. H.; Ha, S. Y.; Chen, G. Q.; Kentish, S. E.; Yeo, J.-G. Assessment of Membrane Performance for Post-Combustion CO<sub>2</sub> Capture. *Ind. Eng. Chem. Res.* **2022**, *61* (1), 777–785.
- (4) Zhang, M.; Chen, L.; Yuan, Z.; Semiat, R.; He, X. CO<sub>2</sub>-Philic Imidazolium-Based Poly(Ionic Liquid) Composite Membranes for Enhanced CO<sub>2</sub>/N<sub>2</sub> Separation. *Ind. Eng. Chem. Res.* **2023**, *62* (22), 8902–8910.
- (5) Liu, Z.; Deng, Z.; Davis, S.; Ciais, P. Monitoring global carbon emissions in 2022. *Nat. Rev. Earth Environ.* **2023**, *4* (4), 205–206.
- (6) Scofield, J. M. P.; Gurr, P. A.; Kim, J.; Fu, Q.; Kentish, S. E.; Qiao, G. G. Blends of Fluorinated Additives with Highly Selective Thin-Film Composite Membranes to Increase CO<sub>2</sub> Permeability for CO<sub>2</sub>/N<sub>2</sub> Gas Separation Applications. *Ind. Eng. Chem. Res.* **2016**, *55* (30), 8364–8372.

- (7) Kwak, N.-S.; Lee, J. H.; Lee, I. Y.; Jang, K. R.; Shim, J.-G. A study of the CO<sub>2</sub> capture pilot plant by amine absorption. *Energy* **2012**, *47* (1), 41–46.
- (8) Hospital-Benito, D.; Lemus, J.; Moya, C.; Santiago, R.; Paramio, C.; Palomar, J. Aspen plus supported design of pre-combustion CO<sub>2</sub> capture processes based on ionic liquids. *Sep. Purif. Technol.* **2022**, *290*, No. 120841.
- (9) Kessler, E.; Ninni, L.; Breug-Nissen, T.; Willy, B.; Schneider, R.; Irfan, M.; Rolker, J.; von Harbou, E.; Hasse, H. Thermodynamic Properties of a System for CO<sub>2</sub> Absorption with Liquid–Liquid Phase Split: EvA<sub>25</sub> + H<sub>2</sub>O + CO<sub>2</sub>. *Ind. Eng. Chem. Res.* **2022**, *61* (41), 15289–15300.
- (10) Rehman, A.; Heo, Y.-J.; Nazir, G.; Park, S.-J. Solvent-free, one-pot synthesis of nitrogen-tailored alkali-activated microporous carbons with an efficient CO<sub>2</sub> adsorption. *Carbon* **2021**, *172*, 71–82.
- (11) Raganati, F.; Chirone, R.; Ammendola, P. CO<sub>2</sub> Capture by Temperature Swing Adsorption: Working Capacity As Affected by Temperature and CO<sub>2</sub> Partial Pressure. *Ind. Eng. Chem. Res.* **2020**, *59* (8), 3593–3605.
- (12) Maqsood, K.; Mullick, A.; Ali, A.; Kargupta, K.; Ganguly, S. Cryogenic carbon dioxide separation from natural gas: a review based on conventional and novel emerging technologies. *Rev. Chem. Eng.* **2014**, *30* (5), 453–477.
- (13) Zeng, P.; Zhao, C.; Liang, C.; Li, P.; Zhang, H.; Wang, R.; Guo, Y.; Xia, H.; Sun, J. Comparative study on low-temperature CO<sub>2</sub> adsorption performance of metal oxide-supported, graphite-casted K<sub>2</sub>CO<sub>3</sub> pellets. *Sep. Purif. Technol.* **2023**, *306*, No. 122608.
- (14) Gao, X.; Lu, K.; Yang, Y.; Cheng, Q.; Wang, Z. A novel economical reactive distillation with two reaction sections for separating isobutene in C<sub>4</sub> to save energy and reduce CO<sub>2</sub> emissions. *Sep. Purif. Technol.* **2023**, *306*, No. 122723.
- (15) Otani, A.; Zhang, Y.; Matsuki, T.; Kamio, E.; Matsuyama, H.; Maginn, E. J. Molecular Design of High CO<sub>2</sub> Reactivity and Low Viscosity Ionic Liquids for CO<sub>2</sub> Separative Facilitated Transport Membranes. *Ind. Eng. Chem. Res.* **2016**, *55* (10), 2821–2830.
- (16) Dai, Y.; Niu, Z.; Luo, W.; Wang, Y.; Mu, P.; Li, J. A review on the recent advances in composite membranes for CO<sub>2</sub> capture processes. *Sep. Purif. Technol.* **2023**, *307*, No. 122752.
- (17) Li, H.; Haas-Santo, K.; Schygulla, U.; Dittmeyer, R. Inorganic microporous membranes for H<sub>2</sub> and CO<sub>2</sub> separation—Review of experimental and modeling progress. *Chem. Eng. Sci.* **2015**, *127*, 401–417.
- (18) Aydani, A.; Maghsoudi, H.; Brunetti, A.; Barbieri, G. Silica sol gel assisted defect patching of SSZ-13 zeolite membranes for CO<sub>2</sub>/CH<sub>4</sub> separation. *Sep. Purif. Technol.* **2021**, *277*, No. 119518.
- (19) Thür, R.; Van Havere, D.; Van Velthoven, N.; Smolders, S.; Lamaire, A.; Wieme, J.; Van Speybroeck, V.; De Vos, D.; Vankelecom, I. F. J. Correlating MOF-808 parameters with mixed-matrix membrane (MMM) CO<sub>2</sub> permeation for a more rational MMM development. *J. Mater. Chem. A* **2021**, *9* (21), 12782–12796.
- (20) Vinoba, M.; Bhagiyalakshmi, M.; Alqaheem, Y.; Alomair, A. A.; Pérez, A.; Rana, M. S. Recent progress of fillers in mixed matrix membranes for CO<sub>2</sub> separation: A review. *Sep. Purif. Technol.* **2017**, *188*, 431–450.
- (21) Qin, Z.; Ma, Y.; Wei, J.; Guo, H.; Wang, B.; Deng, J.; Yi, C.; Li, N.; Yi, S.; Deng, Y. et al. Recent progress in ternary mixed matrix membranes for CO<sub>2</sub> separation. *Green Energy Environ.* **2023**.
- (22) Zhang, Z.; Rao, S.; Han, Y.; Pang, R.; Ho, W. S. W. CO<sub>2</sub>-selective membranes containing amino acid salts for CO<sub>2</sub>/N<sub>2</sub> separation. *J. Membr. Sci.* **2021**, *638*, No. 119696.
- (23) Nguyen, T. T. T.; Lin, J.-B.; Shimizu, G. K. H.; Rajendran, A. Separation of CO<sub>2</sub> and N<sub>2</sub> on a hydrophobic metal organic framework CALF-20. *Chem. Eng. J.* **2022**, *442*, No. 136263.
- (24) Zhang, X.; Jiao, C.; Li, X.; Song, X.; Plisko, T. V.; Bilyukovich, A. V.; Jiang, H. Zn ion-modulated polyamide membrane with enhanced facilitated transport effect for CO<sub>2</sub> separation. *Sep. Purif. Technol.* **2022**, *292*, No. 121051.
- (25) Dai, Z.; Ansaldi, L.; Ryan, J. J.; Spontak, R. J.; Deng, L. Nafion/IL hybrid membranes with tuned nanostructure for enhanced CO<sub>2</sub> separation: effects of ionic liquid and water vapor. *Green Chem.* **2018**, *20* (6), 1391–1404.
- (26) Tan, K.; Nijem, N.; Gao, Y.; Zuluaga, S.; Li, J.; Thonhauser, T.; Chabal, Y. J. Water interactions in metal organic frameworks. *CrystEngComm* **2015**, *17* (2), 247–260.
- (27) Canivet, J.; Fateeva, A.; Guo, Y.; Coasne, B.; Farrusseng, D. Water adsorption in MOFs: fundamentals and applications. *Chem. Soc. Rev.* **2014**, *43* (16), 5594–5617.
- (28) Low, J. J.; Benin, A. I.; Jakubczak, P.; Abrahamian, J. F.; Faheem, S. A.; Willis, R. R. Virtual High Throughput Screening Confirmed Experimentally: Porous Coordination Polymer Hydration. *J. Am. Chem. Soc.* **2009**, *131* (43), 15834–15842.
- (29) Chiu, N. C.; Loughran, R. P.; Gladysiak, A.; Vismara, R.; Park, A.-H. A.; Stylianou, K. C. Wet flue gas CO<sub>2</sub> capture and utilization using one-dimensional metal–organic chains. *Nanoscale* **2022**, *14* (40), 14962–14969.
- (30) Yu, J.; Xie, L.-H.; Li, J.-R.; Ma, Y.; Seminario, J. M.; Balbuena, P. B. CO<sub>2</sub> Capture and Separations Using MOFs: Computational and Experimental Studies. *Chem. Rev.* **2017**, *117* (14), 9674–9754.
- (31) Yang, F.; Ge, T.; Zhu, X.; Wu, J.; Wang, R. Study on CO<sub>2</sub> capture in humid flue gas using amine-modified ZIF-8. *Sep. Purif. Technol.* **2022**, *287*, No. 120535.
- (32) Lai, Q.; Chu, Z.-Q.; Xiao, X.; Dai, D.; Song, T.; Luo, T.-Y.; Tang, W.; Feng, X.; Zhang, Z.; Li, T.; et al. Two-dimensional Zr/Hf-hydroxamate metal–organic frameworks. *Chem. Commun.* **2022**, *58* (22), 3601–3604.
- (33) Feng, X.; Qin, Z.; Lai, Q.; Zhang, Z.; Shao, Z.-W.; Tang, W.; Wu, W.; Dai, Z.; Liu, C. Mixed-matrix membranes based on novel hydroxamate metal–organic frameworks with two-dimensional layers for CO<sub>2</sub>/N<sub>2</sub> separation. *Sep. Purif. Technol.* **2023**, *305*, No. 122476.
- (34) Deng, J.; Dai, Z.; Deng, L. Effects of the Morphology of the ZIF on the CO<sub>2</sub> Separation Performance of MMMs. *Ind. Eng. Chem. Res.* **2020**, *59* (32), 14458–14466.
- (35) Wei, J.; Ma, Y.; Qin, Z.; Jin, Z.; Jin, Y.; Yang, L.; Yao, L.; Jiang, W.; Deng, Y.; Huang, Y.; et al. Membrane fabricated via a facile non-solvent induced microstructure re-arrangement with superior CO<sub>2</sub> separation performances. *Sep. Purif. Technol.* **2023**, *320*, No. 124182.
- (36) Yang, H.; Liang, S.; Zhang, P.; Zhang, X.; Lu, P.; Liu, Y.; Cao, X.; Li, Y.; Wang, Q. Improved CO<sub>2</sub> separation performance of mixed matrix membranes via expanded layer double hydroxides and methanol post-treatment. *J. Membr. Sci.* **2023**, *670*, No. 121345.
- (37) Kim, K.; Ingole, P. G.; Kim, J.; Lee, H. Separation performance of PEBAK/PEI hollow fiber composite membrane for SO<sub>2</sub>/CO<sub>2</sub>/N<sub>2</sub> mixed gas. *Chem. Eng. J.* **2013**, *233*, 242–250.
- (38) Higgins, F. S.; Magliocco, L. G.; Colthup, N. B. Infrared and Raman Spectroscopy Study of Alkyl Hydroxamic Acid and Alkyl hydroxamate Isomers. *Appl. Spectrosc.* **2006**, *60* (3), 279–287.
- (39) Li, G.; Kujawski, W.; Knozowska, K.; Kujawa, J. Thin Film Mixed Matrix Hollow Fiber Membrane Fabricated by Incorporation of Amine Functionalized Metal-Organic Framework for CO<sub>2</sub>/N<sub>2</sub> Separation. *Materials* **2021**, *14* (12), 3366.
- (40) Rajati, H.; Navarchian, A. H.; Rodrigue, D.; Tangestaninejad, S. Improved CO<sub>2</sub> transport properties of Matrimid membranes by adding amine-functionalized PVDF and MIL-101(Cr). *Sep. Purif. Technol.* **2020**, *235*, No. 116149.
- (41) Mohammed, S. A.; Nasir, A. M.; Aziz, F.; Kumar, G.; Sallehuddin, W.; Jaafar, J.; Lau, W. J.; Yusof, N.; Salleh, W. N. W.; Ismail, A. F. CO<sub>2</sub>/N<sub>2</sub> selectivity enhancement of PEBAK MH 1657/Aminated partially reduced graphene oxide mixed matrix composite membrane. *Sep. Purif. Technol.* **2019**, *223*, 142–153.
- (42) Gou, M.; Zhu, W.; Sun, Y.; Guo, R. Introducing two-dimensional metal-organic frameworks with axial coordination anion into PEBAK for CO<sub>2</sub>/CH<sub>4</sub> separation. *Sep. Purif. Technol.* **2021**, *259*, No. 118107.
- (43) Meshkat, S.; Kaliaguine, S.; Rodrigue, D. Enhancing CO<sub>2</sub> separation performance of PEBAK® MH-1657 with aromatic carboxylic acids. *Sep. Purif. Technol.* **2019**, *212*, 901–912.

- (44) Zhao, D.; Ren, J.; Wang, Y.; Qiu, Y.; Li, H.; Hua, K.; Li, X.; Ji, J.; Deng, M. High CO<sub>2</sub> separation performance of PEBA<sup>®</sup>/CNTs/GTA mixed matrix membranes. *J. Membr. Sci.* **2017**, *521*, 104–113.
- (45) Li, L.; Wang, J.; Li, H.; Guan, X.; Li, K.; Zhang, B.; Li, X.; Zhang, J. Constructing multi-dimensional transport pathways by mixed-dimensional fillers in membranes for efficient CO<sub>2</sub> separation. *J. Environ. Chem. Eng.* **2023**, *11* (1), No. 109178.
- (46) Wu, C.; Guo, H.; Liu, X.; Zhang, B. Mixed matrix membrane comprising glycine grafted CuBTC for enhanced CO<sub>2</sub> separation performances with excellent stability under humid atmosphere. *Sep. Purif. Technol.* **2022**, *295*, No. 121287.
- (47) Zhu, W.; Wang, L.; Cao, H.; Guo, R.; Wang, C. Introducing defect-engineering 2D layered MOF nanosheets into PEBA<sup>®</sup> matrix for CO<sub>2</sub>/CH<sub>4</sub> separation. *J. Membr. Sci.* **2023**, *669*, No. 121305.
- (48) Kanehashi, S.; Chen, G. Q.; Ciddor, L.; Chaffee, A.; Kentish, S. E. The impact of water vapor on CO<sub>2</sub> separation performance of mixed matrix membranes. *J. Membr. Sci.* **2015**, *492*, 471–477.
- (49) Wei, J.; Ma, Y.; Qin, Z.; Jin, Z.; Jin, Y.; Yang, L.; Yao, L.; Jiang, W.; Deng, Y.; Huang, Y.; et al. Membrane fabricated via a facile non-solvent induced microstructure re-arrangement with superior CO<sub>2</sub> separation performances. *Sep. Purif. Technol.* **2023**, *320*, No. 124182.
- (50) Park, T.; Chung, E. Low-pressure plasticization of PEBA<sup>®</sup> 2533 membrane by carbon dioxide. *Asia-Pac. J. Chem. Eng.* **2023**, *18* (3), No. e2902.
- (51) Gao, J.; Mao, H.; Jin, H.; Chen, C.; Feldhoff, A.; Li, Y. Functionalized ZIF-7/PEBA<sup>®</sup> 2533 mixed matrix membranes for CO<sub>2</sub>/N<sub>2</sub> separation. *Microporous Mesoporous Mater.* **2020**, *297*, No. 110030.
- (52) Behroozi, M.; Pakizeh, M. Study the effects of Cloisite15A nanoclay incorporation on the morphology and gas permeation properties of Pebax2533 polymer. *J. Appl. Polym. Sci.* **2017**, *134* (37), 45302.
- (53) Ehsani, A.; Pakizeh, M. Synthesis, characterization and gas permeation study of ZIF-11/PEBA<sup>®</sup> 2533 mixed matrix membranes. *J. Taiwan Inst. Chem. Eng.* **2016**, *66*, 414–423.
- (54) Rahman, M. M.; Filiz, V.; Shishatskiy, S.; Abetz, C.; Neumann, S.; Bolmer, S.; Khan, M. M.; Abetz, V. PEBA<sup>®</sup> with PEG functionalized POSS as nanocomposite membranes for CO<sub>2</sub> separation. *J. Membr. Sci.* **2013**, *437*, 286–297.
- (55) Hasan, M. R.; Zhao, H.; Steunou, N.; Serre, C.; Malankowska, M.; Téllez, C.; Coronas, J. Optimization of MIL-178(Fe) and PEBA<sup>®</sup> 3533 loading in mixed matrix membranes for CO<sub>2</sub> capture. *Int. J. Greenh. Gas Control* **2022**, *121*, No. 103791.
- (56) Wang, D.; Yao, D.; Wang, Y.; Wang, F.; Xin, Y.; Song, S.; Zhang, Z.; Su, F.; Zheng, Y. Carbon nanotubes and graphene oxide-based solvent-free hybrid nanofluids functionalized mixed-matrix membranes for efficient CO<sub>2</sub>/N<sub>2</sub> separation. *Sep. Purif. Technol.* **2019**, *221*, 421–432.